Available online at www.sciencedirect.com
SCIENCE DIRECT®
C. R. Chimie 8 (2005) 1946–1953
COMPTES RENDUS CHIMIE
http://france.elsevier.com/direct/CRAS2C/

Preliminary communication / Communication

One-pot synthesis of fluorescent porous aluminosilicate nanoparticles

Élisabeth Gavilan, Tristan Doussineau, Abdelslam El Mansouri, Monique Smaïhi *, Sébastien Balme, Jean-Marc Janot

IEM UMR 5635, CNRS, 1919, route de Mende, 34293 Montpellier cedex 5, France

Received 8 February 2005; accepted after revision 26 April 2005

Available online 14 July 2005

Abstract

Fluorescent mesoporous aluminosilicates nanoparticles were synthesized in one-pot procedure from precursors AlOiPr/TEOS/TEAOH in presence of Rhodamine B. They exhibit interesting mesoporous properties with narrow pore size distribution as well as excellent thermal and chemical stability. ***To cite this article: E. Gavilan et al., C. R. Chimie (8) 2005***.

Résumé

Des aluminosilicates fluorescents et mésoporeux ont été préparés sous la forme de nanoparticules par une procédure en une étape à partir des précurseurs isopropoxyde d'aluminium/tetraéthoxysilane/hydrodroxyde de tétraéthylammonium (AlOiPr/TEOS/TEAOH) en présence de Rhodamine B. Leur morphologie, structures poreuse et moléculaire ont été caractérisées par microposcopie électronique à balayage, adsorption–désorption de gaz et résonance magnétique nucléaire. La concentration de chromophore introduite dans les particules colloïdales a été obtenue par analyse élémentaire. Finalement, les propriétés optiques statiques et dynamiques ont été étudiées par spectroscopie de fluorescence et mesure de durée de vie des états excités. Ces matériaux présentent des propriétés intéressantes de mésoporosité, avec une distribution de taille de pore étroite ainsi qu'une très bonne stabilité thermique et chimique. Les résultats obtenus par spectroscopie de fluorescence ainsi que les valeurs des durées de vie mettent en évidence le confinement des chromophores dans le solide. Ces propriétés optiques et chimiques permettent d'envisager pour ces matériaux des utilisations en tant que traceur. ***Pour citer cet article : E. Gavilan et al., C. R. Chimie (8) 2005***.

Keywords: Nanoparticles; Mesoporous materials; Aluminosilicates; Fluorescence

Mots clés : Nanoparticules ; Matériaux mésoporeux ; Aluminosilicates ; Fluorescence

* Corresponding author.
E-mail address: smaihi@iemm.univ-montp2.fr (M. Smaïhi).

1631-0748/$ - see front matter © 2005 Académie des sciences. Published by Elsevier SAS. All rights reserved.
doi:10.1016/j.crci.2005.05.004

1. Introduction

The production of particles with a specific size and morphology is of primary importance for the development of new materials. Over the past decade, the importance of materials with length scale of the order of 1–100 nm has been recognized in a broad range of technologies.

Of particular interest are porous nanostructures due to their potential applications, for example in drug storage and release [1–4] biomedical applications [5] optical waveguides [6,7] confined-space catalysis [8,9] and separation [10–12] or low *k* dielectric fillers [13].

The diversity in applications is obtained by incorporation of organic moieties in the porosity. Two procedures can be used for this loading: a post-synthesis treatment or the in situ incorporation of the organic molecules into the structure during the synthesis.

The most advantage of in situ encapsulation of organic molecules in the nanoparticles structure is their homogeneous dispersion and their low migration, aggregation and leakage. In general, encapsulation implies that a stabilizing effect exists since the reactive sites are protected from deactivation and leaching effects. The immobilized species display structural integrity, even under harsh conditions and the composites are easier to handle than their homogeneous counterparts. This means that the resulting structures offer enormous potential for advanced applications in the field of materials science. For example, for biomedical applications, by using dye doped nanoparticles as fluorescent markers, highly sensitive target detection can be achieved, opening the possibility for the fabrication of truly smart bioprobes and biosensors. Compared with conventional fluorescent labeling which is based on single molecules, the bioconjugated nanoparticles that gather thousands of dye molecules in each particle are extremely bright.

The preparation of hollow nanoparticles often involves a first synthesis step based on supramolecular templating of structures [5,14]. Accessibility to the porosity is obtained by a second treatment, which consists on the removal of the structure directing agents (SDA). This is done either by high temperature calcinations or solvent extraction. In case of nanoparticles, these last treatments may lead to irreversible particles aggregation [15,16] and modification of the particles surface properties. In addition, the calcination procedure would destroy any previous grafted organic molecules and the solvent extraction may damage the properties of the in situ encapsulated organic moieties. So far only a few examples of relatively hydrothermally stable porous materials were reported [17].

Therefore, in case of encapsulation of sensitive organic molecules, there is a need in synthesis procedures leading to hybrid porous nanoparticles with a minimum of synthetic steps and no surfactant removal step.

In this paper, we report a simple one-pot method to synthesize stable mesoporous aluminosilicate nanoparticles containing rhodamine B (RhB) fluorescent dyes.

2. Experimental

2.1. Materials preparation

Colloidal mesoporous aluminosilicate nanoparticles with Si/Al ratio of 18.5 were synthesized under mild hydrothermal conditions from a colloidal zeolite beta starting solution containing (0.125–0.25)RhB: $2.25(TEA)_2O{:}0.5Al_2O_3{:}25SiO_2{:}300H_2O$, where TEA is tetraethylammonium hydroxide (TEAOH) (Fluka, 20% in water). Two RhB/Si molar ratios were used for the preparation of these, i.e. 10^{-2} and 5×10^{-3}. Typically, the synthesis route was as follows: Solution A was prepared by adding TEAOH and RhB to aluminium isopropoxide (AlO^iPr). Solution B was prepared by adding TEAOH and RhB to tetraethyl orthosilicate (TEOS) with stirring. Solution A and B were mixed vigorously for 15 min and the resulting solution was transferred in a Teflon lined autoclave. The synthesis was then performed at 100 °C for 2 and 7 days. These synthesis conditions should not damage the chromophore since RhB fusion temperature is about 180 °C and the molecule can withstand pH values up to 12. RhB is characterized by a free carboxyl group. From its pK_a value of 3.1–3.5, it follows that this dye exists as zwitterions during the synthesis [18–20]. Moreover, a positive charge at the chromophore is, in any case, favorable for crystallization inclusion [21]. As reference, samples were prepared without adding the dye in the starting solutions.

The colloidal mesoporous aluminosilicate nanoparticles were purified by five series of high-speed centrifugation (12 000 rpm, 20 min) and re-dispersion in

water or ethanol. The obtained colloidal suspensions were adjusted to a 4 wt.% concentration. For powder characterizations, the recovered solid was dried at 80–100 °C overnight.

Stability of the hybrid materials was evaluated by exposure of the particles to aqueous acetic acid (50% water) at 80 °C for 12 h. After this treatment, the solid was washed by repeated centrifugation (three times, 12,000 rpm) and re-dispersion by ultrasonication. A dispersible powder was obtained after drying at 80–100 °C overnight.

2.2. Sample characterizations

Scanning Electron micrographs were obtained on a Hitachi S-4500 microscope. All samples were platinum coated (2–3 nm) and mounted on aluminum mounts with carbon conducting tape. X-ray diffraction measurements were performed with a Bruker diffractometer D-5000 (Cu $K\alpha_1$ radiation = 0.154 nm).

^{29}Si CP-MAS NMR spectra of the solid samples were recorded on a Bruker spectrometer at 79.49 MHz using 5-μs single pulses (60° flip angle) with 10-s repetition rate and 15-ms contact time employing magic angle spinning at 3.5 kHz; 10 000 scans were accumulated. ^{27}Al MAS-NMR spectra were measured at 104.26 MHz using single pulses of 1-μs duration with a 1 s repetition rate and employing magic angle spinning at 10 kHz; 512 scans were accumulated. All ^{27}Al and ^{29}Si chemical shifts were referenced to 1% aqueous $Al(H_2O)_6^{3+}$ solution and tetramethylsilane (TMS), respectively. The powder samples were filled into 4 mm diameter zirconia rotors.

Dynamic light scattering (DLS) results were obtained using an argon laser (Spectra Physics Series 2000) operating at 632.8 nm. Light scattering measurements were made at 25 ± 0.1 °C.

Static fluorescence spectra were recorded using a Spex Fluorolog 1681 spectrofluorimeter (scanning rate of 2 nm s^{-1}).

Time resolved fluorescence data were obtained by the technique of time correlated single photon counting. The excitation wavelength was obtained using a 82-MHz-mode locked argon ion laser (Spectra Physics model 2030) pumping synchronously a cavity dumped rhodamine 6G dye laser (Spectra Physics model 375 dye laser and 344 cavity dumper). The pulses excitation duration is estimated for such a device around 20 ps (FWHM). Fluorescence decays, obtained after vertically polarized excitation, were collected through a polarizer set to the magic angle (54°73′) using a double monochromator Jobin-Yvon DH10 and a photomultiplier tube Hamamatsu H5323 (Cathode S20, TTS 160 ps). The measured instrumental response function, limited by the PM tube was 160 ps FWHM. The excitation frequency was set to 800 KHz and the count rate limited to 12 KHz. In such condition monoexponential decays were collected for our usual standard (Alexa 594, sulforhodamine 640).

Decay analysis was performed using a Levenberg–Marquardt algorithm. Lifetimes were calculated by iterative adjustment after convolution of the pump profile (scattered light) with a sum of exponentials. We assumed a Poissonnian distribution of counts in the calculation of the χ^2 criterion used to estimate the quality of the adjustment.

Gas sorption experiments were performed by using a Micromeritics ASAP 2010. Nitrogen was used as the adsorbate at 77 K. Samples were outgassed at 80 °C in dynamic vacuum (3×10^{-6} bar) before the adsorption. This outgassing treatment, selected upon considering thermogravimetric results, does not remove the organics from the sample.

Elemental analysis were done by the 'Laboratoire central d'analyses du CNRS' at Vernaison (France).

3. Results

3.1. Materials structure

3.1.1. Morphology

The size and shape of the particles in the samples investigated with SEM (Fig. 1) are very homogeneous with respect to morphology. The size of the particles determined from the SEM images is approximately 170 nm in diameter. This is confirmed by the particles radius measured in the final colloidal suspensions by DLS. This value does not vary drastically with the dye/Si molar ratio of the starting solution. Monomodal particle size distribution is observed with a mean diameter of about 170 nm. The reference sample prepared without the dye gives similar size distribution showing that the presence of a dye in the starting solution does not provoke additional aggregation. These colloidal properties are maintained for all samples even after an

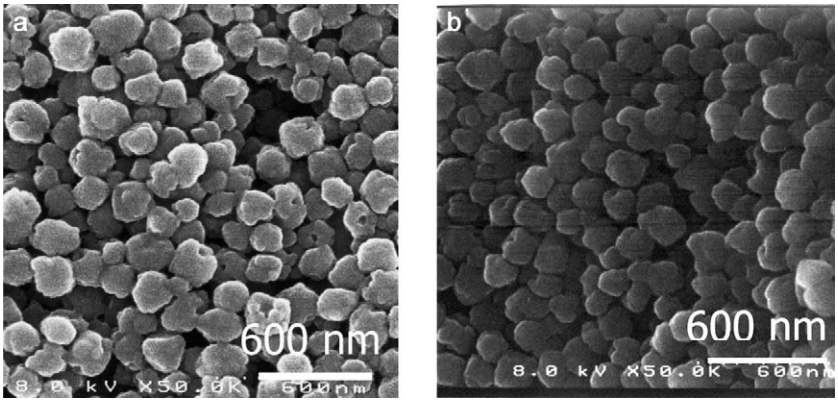

Fig. 1. SEM micrographs of RhB loaded samples: initial dye loading (**a**) 0.3, (**b**) 3.

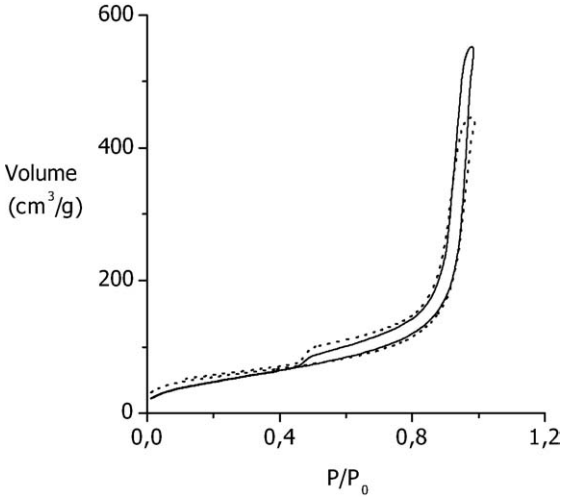

Fig. 2. N_2 adsorption/desorption isotherms of as-synthesized sample 3 (solid line) and after submission to acidic hydrothermal treatment (dotted line).

extensive acidic hydrothermal treatment. The same size distribution is measured before and after an acidic treatment.

N_2-adsorption/desorption isotherms obtained for these materials confirm the mesoporous structure of these samples (Fig. 2). The dye-loaded samples present type IV isotherms (definition by IUPAC) [22] which are characteristic of mesoporous materials while the reference material exhibits a N_2-adsorption/desorption isotherm corresponding to typical non-porous solids (low surface area and no specific mesopore distribution). The appearance of hysteresis loops in the dye-loaded samples isotherms may indicate the presence of 'ink-bottle'-type pores in the aluminosilicate materials [23]. The specific surface area is about 200 $m^2\ g^{-1}$ and the materials exhibit a pore size distribution (calculated from the desorption branch) over a relatively narrow range from 8 to 20 nm. Table 1 reports the textural properties of the samples obtained after different hydrothermal treatment duration as well as with various RhB/Si molar ratios in the starting solution. The data are reported from the N_2 isotherms with the total pore volume and the BJH mesopore size obtained from the des-

Table 1
Textural properties of dye-loaded nanoparticles, as-synthesized and after exposure to acidic hydrothermal treatment

Sample treatment	Initial dye loading ($\mu mol\ g^{-1}$)	Langmuir specific area (m^2)	Pore radius (nm)	Pore volume ($cm^3\ g^{-1}$)
Hydrothermal 100 °C, 7 days	0	91	6.2	0.15
	0.3	156	7.3	0.78
	3	164	7	0.7
Hydrothermal 100 °C, 2 days	0.3	200	7.2	0.8
	3	213	7.1	0.8
Acidic exposure after 80 °C, 12 h	0.3	207	7.5	0.81
	3	190	6.3	0.62

orption leg at $P/P_0 = 0.8–0.9$. Whatever the dye loading, these textural properties are not drastically modified after an extensive acidic hydrothermal treatment. Exposure to 1-M aqueous acetic acid at 80 °C for 12 h. resulted in negligible structural degradation (Fig. 2, Table 1).

3.1.2. Crystallinity

From a crystalline point of view, samples prepared without RhB in the starting solution are fully crystalline with a zeolite BEA-type structure, after a hydrothermal treatment of 7 days at 100 °C. However, the same hydrothermal treatment in presence of RhB, leads to powder X-ray diffraction patterns of the dye-loaded samples with a broad band centered at 22° (2θ), characteristic of amorphous silicates, and weak diffraction peaks superimposed suggesting the presence of some zeolite Beta seeds in the solid. A shorter hydrothermal treatment (2 days) makes the weak diffraction peaks disappear and only the broad band appears in the powder X-ray diffraction patterns of the dye-loaded samples. The absence of a low angle peak in the 2θ range from 1° to 3°, which is a characteristic of ordered mesoporous materials, indicates that there is no long-range order in these materials. No modification of these structural properties is observed after an acidic hydrothermal treatment. However, the modification of the XRD patterns of the material after addition of the dye in the starting solution suggests that the dye influences strongly the mechanisms of the solid structuration. It has been already observed that addition or even slight concentration modification of an organic molecule in mesoporous materials starting solution provokes dramatic changes in the final structure of the material [24]. These structural modifications upon RhB addition in the starting solution also suggest the existence of strong interactions between the dye molecule and the soluble aluminosilicate precursors. This has been already observed in the solid state, since several studies have been devoted on the interaction of Rhodamine dyes with silica surfaces, which are supposed to interact with the polar surface through hydrogen bonding interactions [25,26].

3.1.3. Molecular structure

Solid-state NMR enables to obtain the information on the short-range coordination environment of the structuring atoms (silicon and aluminium) of the samples. Identical coordination environments are observed for all dye-loaded samples, the reference sample and the samples submitted to the acidic hydrothermal treatment. The ^{27}Al MAS-NMR spectra present a single signal at 52 ppm, which is assigned, to tetrahedral $Al(OSi)_4$ groups (Fig. 3). This is characteristic of aluminosilicate frameworks and presages the presence of a high fraction of Brønstedt acid sites. The ^{29}Si CP-MAS NMR spectra exhibit two resonances at –110 and –100 ppm, indicating the presence of Q^4 species in which all of the oxygen atoms are bridging and Q^3 sites, which bear a single hydroxy group (Fig. 4). Thus from a structural point of view, results obtained by XRD and NMR show that the dye-loaded sample structure is maintained after an acidic hydrothermal treatment.

3.1.4. Dye concentration

The quantification of the dye loading as well as the Si/Al ratio and the TEAOH concentration in the materials after synthesis was obtained by elemental analysis (Table 2). These data enable the evaluation of the influence of the dye concentration as well as the hydrothermal treatment duration on the final materials composition.

First, the TEAOH concentration in the dye-loaded materials is significantly decreased when compared to the dye-free reference sample. For similar hydrother-

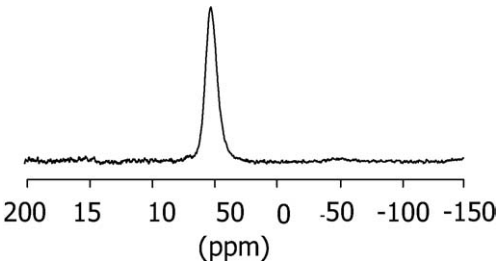

Fig. 3. ^{27}Al MAS-NMR spectrum of sample with RhB initial loading 3 μmol g^{-1}.

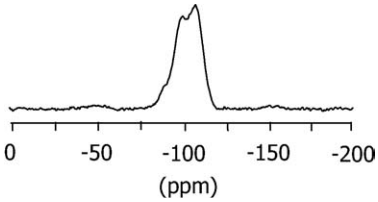

Fig. 4. ^{29}Si CP-MAS NMR spectrum of sample with RhB initial loading 3 μmol g^{-1}.

Table 2
Chemical composition (calculated from elemental analysis results) of the reference and dye-loaded samples obtained after various thermal treatments

Hydrothermal treatment duration	Initial RhB loading (μmol g^{-1})	Si/Al molar ratio	TEAOH/Si molar ratio	Final RhB loading[a] (μmol g^{-1})
2 days	0.3	23.1	0.03	0.05
	3	18.8	0.01	0.5
7 days	0	25.6	0.11	–
	0.3	20.3	0.06	0.05
	3	18.1	0.06	0.5

[a] Calculated from elemental analysis.

mal duration treatment, dye-loaded samples contain half-less template molecules than the reference dye-free sample. XRD experiments have shown the dramatic influence of the presence of a dye in the starting solutions on the sample crystallinity suggesting the presence of strong interactions between the silicate molecular precursors and the dye. Elemental analysis data confirms the presence of strong interactions between the silicate molecular precursors and the dye, which may inhibit the incorporation of as many template molecules in the structure as in the reference sample.

On the other hand, the RhB concentration in the material is not dramatically modified by the initial RhB concentration in the starting solution neither by the duration of the hydrothermal treatment. The maximum loading of RhB, which can be obtained in those samples corresponds to a RhB/Si molar ratio of approximately 4.5×10^{-3}.

A significant decrease of the Si/Al ratio is observed with the increase of the RhB loading. Although major reductions are often observed between initial and final Al concentrations in hydrothermally prepared solids [27], no clear interpretation has been given to these variations.

3.1.5. Photophysical properties

Finally, spectrofluorimetric measurements were made to characterize the optical properties of these particles (Fig. 5). When excited at 540 nm, the excitation spectra display almost the same profile for all the samples whatever their dye concentration and their hydrothermal treatment duration. However, while in aqueous TEAOH and ethanolic solutions, the RhB maximum emission peak is located at 592 nm, the emission peak of the dye-loaded particles were blue-shifted to 577 nm (Fig. 5). This is a characteristic behavior of confined dyes, which indicates the presence of additional interactions of the dye with its environment compared to its mean free path in solution. This shows also that the dye molecules in the dye-loaded nanoparticles, are located in the aluminosilicate framework instead of adsorbed at the particles surface. Moreover, after an extensive acidic hydrothermal treatment, the dye-loaded samples still present a fluorescence emission spectrum, which is similar to the non-treated, samples spectra wit a small red-shift of few nanometers (Fig. 5). This small shift may be due to the modification of the surface species of the inorganic network. Nevertheless, the similarity of the emission wavelength before and after the acidic treatment demonstrates the photostability of these samples. Moreover, this demonstrates also the presence of strong interactions between the dye and the aluminosilicate framework and confirms that the location of the dye molecule is inside the frame-

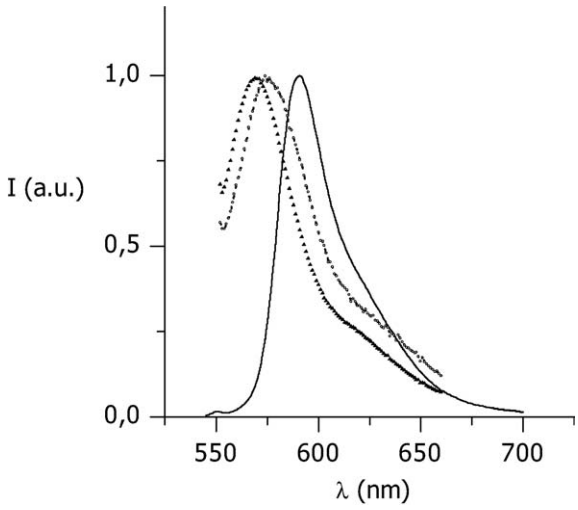

Fig. 5. Fluorescence emission spectra of sample loaded with RhB (initial loading 3 μmol g^{-1}) after synthesis (triangles), after acidic exposure (dotted line) and RhB in TEAOH solution (2.5×10^{-6} M) (solid line). λ_{excit} = 543 nm.

work (otherwise the acidic treatment would have desorbed the adsorbed dye molecules).

In order to fully characterize the optical properties of these samples, the emission lifetime was measured for all dye-loaded samples at 19 °C with excitation at 590 and 610 nm emission. In solution, free-RhB traces exhibit monoexponential behavior of the decay with associated lifetimes of ~1.6 ns. For the zeolite entrapped dye, it is necessary to apply a biexponential model of the decay to reproduce the observed decay curve. For RhB loaded zeolite nanoparticles, the rhodamine lifetime was around 3.9 ns with a second component (~1.45 ns) contributing approximately 9% of the initial emission intensities. A single lifetime denotes a very homogeneous environment around the dye molecules (heterogeneous environments yield multiple lifetimes [28]). This behavior, also observed for other dye-loaded zeolites [29], may arise from the contribution from small fraction (~6%) of interacting adjacent cage pairs [30]. These values are in agreement with previous measurements reported for fluorescence lifetime of RhB in silica matrix (3.58 ns [28]). It has been also assumed that the decreased lifetime may result from interactions with the silanols instead of dye–dye interactions. [31] However, a higher lifetime value than the lifetime observed in ethanol/water dye solution denotes a more rigid environment for the dye molecule, which prevents the free arrangement of the molecules. Thus, the dramatic increase of the lifetime value observed for the dyes-loaded nanoparticles accounts for their entrapment in the cages of the inorganic host.

4. Conclusion

Fluorescent porous aluminosilicate nanoparticles have been prepared by a one-pot synthesis procedure. This procedure has been exemplified for RhB dye molecule and can be extended to other chromophoric molecules. It preserves the ability of the entrapped chromophore for fluorescence even after an extensive acidic treatment. This chemical stability has been attributed to strong interactions of the chromophore with the inorganic aluminosilicate species present in the starting solution. These interactions lead to a dramatic modification in the solid structuration during the hydrothermal treatment and also provoke large Stokes shifts in the fluorescence spectra. The increase of the emission's lifetime observed between the RhB dye in solution and in the dye-loaded nanoparticles accounts for their stabilization and random distribution in the solid, which behaves like a solid solvent.

Acknowledgments

Funding of this work by the Ministère Délégué à la Recherche (ACI Nanosciences 045 270 and 042 130) is gratefully acknowledged.

References

[1] J.H. Fendler, Nanoparticles and Nanostructured Films, Wiley-VCH, Weinheim, Germany, 1998.
[2] T.M.S. Chang, Microencapsulation (Artificial Cells), in: J.C. Salamone (Ed.), Polymeric Materials Encyclopedia, vol. 6, CRC Press, New York, 1996, pp. 4351–4355.
[3] H. Huang, E.E. Remsen, T. Kowalewski, K.L. Wooley, J. Am. Chem. Soc. 121 (1999) 3805.
[4] C.-Y. Lai, B.G. Trewyn, D.M. Jeftinija, K. Jeftinija, S. Xu, S. Jeftinija, V.S.-Y. Lin, J. Am. Chem. Soc. 125 (2003) 4451.
[5] A.E. Ostafin, M. Siegel, Q. Wang, H. Mizukami, Micropos. Mesopor, Mater 57 (2003) 47.
[6] S. Sadasivan, D. Kushalani, S. Mann, J. Mater. Chem. 13 (2003) 1023–1029.
[7] S. Mintova, V. De Waele, U. Schmidhammer, E. Riedle, T. Bein, Angew. Chem. Int. Ed. Engl. 42 (2003) 1611–1614.
[8] N.B. Castagnola, P.K. Dutta, J. Phys. Chem. B 102 (1998) 1696–1702.
[9] N.B. Castagnola, P.K. Dutta, J. Phys. Chem. B 105 (2001) 1537–1542.
[10] C.E. Fowler, D. Khushalani, B. Lebeau, S. Mann, Adv. Mater. 13 (2001) 649–652.
[11] Y. Lu, H. Fan, A. Stump, T.L. Ward, T. Rieker, C.J. Brinker, Nature 398 (1999) 13.
[12] Y. Liu, T. Pinnavaia, J. Am. Chem. Soc. 125 (2003) 2376–2377.
[13] H. Fan, F. Van Swol, Y. Lu, C.J. Brinker, J. Non-Cryst. Solids 285 (2001) 71–78.
[14] B.J. Schoeman, J. Sterte, J.-E. Otterstedt, Zeolites 14 (1994) 110.
[15] L.M. Huang, Z.B. Wang, J.Y. Sun, L. Miao, Q.Z. Li, Y. Yan, D.Y. Zha, J. Am. Chem. Soc. 122 (2000) 3530.
[16] B.J. Zhao, S.A. Davis, N.H. Mendelson, S. Mann, Chem. Commun. (2000) 781.
[17] Y. Li, Z. Hua, H. Chen, M. Ruan, D. Yan, Nano Lett. 3 (2003) 609–612.
[18] R.W. Ramette, E.B. Sandell, J. Am. Chem. Soc. 78 (1956) 4872.
[19] I. López Arbeloa, P. Ruiz Ojeda, Chem. Phys. Lett. 79 (1981) 347.

[20] M. El Baraka, M. Deumié, P. Viallet, J. Photochem. Photobiol. A, Chem. 62 (1991) 195.
[21] D. Wörhle, G. Schultz-Ekloff, Adv. Mater. 6 (1994) 875.
[22] S.J. Gregg, K.S.W. Sing, Adsorption, Surface Area and Porosity, second ed., Academic Press, London, 1995.
[23] R. Takahashi, S. Sato, T. Sodesawa, M. Kawakita, M. Ogura, J. Phys. Chem. B 104 (2000) 12184.
[24] M. Huang, F. Kartono, B. Dunn, J. Zink, Chem. Mater. 14 (2002) 5153–5162.
[25] T. Kikteva, D. Star, Z. Zhao, T. Baisley, G. Leach, J. Phys. Chem. B (1999) 103.
[26] L. Vieia Ferreira, M. Lamos, M. Reis, A. Bothelho do Rego, Langmuir 16 (2000) 5673–5680.
[27] B. Gauthier, M. Smaïhi, J. New, Chem. 28 (2004) 457–461.
[28] U. Narand, R. Wang, P.N. Prasad, F.V. Bright, J. Phys. Chem. 98 (1994) 17.
[29] A.A. Bhuiyan, J.R. Kincaid, Inorg. Chem. 38 (1999) 4759–4764.
[30] M. Sykora, J.R. Kincaid, P.K. Dutta, N.B. Castagnola, J. Phys. Chem. 103 (1999) 309.
[31] G. Gu, P.P. Ong, Q.T. Li, J. Phys. D 32 (1999) 2287.